Mesospheric temperature observations at the USU/CASS Atmospheric Lidar Observatory (ALO)

Vincent B. Wickwar, Thomas D. Wilkerson, Marc Hammond, Joshua P. Herron

Center for Atmospheric and Space Sciences, Utah State University
4405 Old Main Hill, Logan, UT 84322-4405, USA

ABSTRACT

The Center for Atmospheric and Space Sciences (CASS) at Utah State University (USU) operates the ALO for studying the middle atmosphere from the stratosphere to the lower thermosphere. ALO's mid-latitude location (41.74°N, 111.81°W, 1466 m) is very unique in that it is in the middle of an extensive set of rugged mountains, the Rocky Mountains, which are a major orographic source of gravity waves that may give rise to a longitudinal variation in the mesospheric structure. Mesospheric observations between approximately 45 and 90 km have been carried out on many clear nights with the ALO Rayleigh-scatter lidar since late 1993. They have been carried out, mostly, with a frequency-doubled Nd:YAG laser producing 18 W at 532 nm and a 44-cm zenith-pointing telescope. To obtain better and more complete observations in the future, a considerably bigger steerable telescope, an alexandrite ring laser for resonance scatter, and an expanded data-acquisition system are being developed. The observations in the extensive existing database have been reduced to provide absolute temperature profiles, which provide important information for understanding the physics and chemistry of the middle atmosphere and for examining global change. They have been used to make a mesospheric temperature climatology that has been and is being used to examine secular, annual, seasonal, and tidal variations, to compare with other temperature observations and with modeled temperatures, and to study mesospheric inversion layers. Day-to-day changes in the temperature profiles are also being compared to meteorological parameters to see if mesospheric changes can be related to low-altitude sources. Temporal and spatial fluctuations in the density profiles have also been examined to provide more direct information on gravity wave activity. And, on 24 June 1999 UT, the lidar probed the first known noctilucent cloud to penetrate to this low latitude, approximately 10° equatorward of previously reported sightings and detections.

Keywords: Lidar, Rayleigh scatter, resonance scatter, middle atmosphere, mesosphere, temperatures, global change, noctilucent clouds, gravity waves, tides

1. INTRODUCTION

Low temperatures in the polar summer mesosphere are understood in terms of the meridional component of the mesospheric circulation. It flows from summer to winter hemisphere at high altitude followed by subsidence heating in the winter hemisphere and flows from winter to summer hemisphere at lower altitudes followed by adiabatic cooling of the rising air in the summer mesosphere. The result of these dynamical effects is that the upper mesospheric temperature at polar latitudes is considerably colder in summer than in winter. The driving force for the mesospheric circulation is attributed to gravity waves generated in the troposphere, propagating upward, and depositing momentum in the mesosphere.

To understand this introduction and see where the research is going, it is necessary to have some background information on the structure and properties of the mesosphere leading up to the edge of space. When mean zonal wind and temperature patterns throughout the region were constructed[1], they showed a stratosphere that was basically in radiative equilibrium (except for the polar winter) and a mesosphere that was not in radiative equilibrium. This manifested itself in two ways: the summer mesopause temperature was much colder than the winter mesopause temperature, and the mesospheric jets (toward the east in winter and toward the west in summer) were much slower than expected. Calculations and modeling showed that substantial agreement could be obtained by introducing a Rayleigh friction term to decelerate the mesospheric jets[2–6]. This produced a meridional circulation from summer to winter that induces vertical motions leading to adiabatic cooling in the summer hemisphere and compressional heating in the winter hemisphere. Meanwhile, the dissipation of vertically propagating gravity waves was proposed as the source of this drag[7,8]. These gravity waves are believed to originate in the troposphere, the most often suggested sources being orography[9,10], convective storms[11,12], and the jet stream[13,14]. However, what is important for this discussion is the existence of these waves, not their source. As they propagate upwards, conservation of energy arguments say that the wave amplitude will grow by a factor of *e* every two-scale heights until energy dissipation (saturation or "breaking") sets in. This growth would be more than two orders of magnitude between the troposphere and the upper mesosphere. It became practical to test the effects of breaking gravity waves, (i.e., eddy forcing) in model calculations after a scheme was proposed for the parameterization of momentum deposition (wave drag) and

turbulent (eddy) diffusion[15]. Several investigators tested the effects of wave drag[16,17]; others tested the combined effects of wave drag and turbulent diffusion[18,19]. The success of these and similar calculations in accounting for the major dynamical features of the mesosphere and for the distribution of minor constituents in the mesosphere (and hence variations in emissions such as OH), have lent strong support to the central role of gravity waves. And it appears that the eddy forcing from these breaking gravity waves accounts for the middle atmosphere circulation and departures from radiative equilibrium.

2. ALO LOCATION

The location of ALO is good for lidar operations and education, lidar observations, correlative observations, and gravity wave studies. The Observatory is located on the USU campus, in the building occupied by both CASS and the Physics Department. This makes it very convenient for students to operate the lidar and to use it for their research.

The location in northern Utah has a high proportion of cloudless nights or nights with only thin cirrus clouds. Furthermore, the air is comparatively clear because the valley where USU is located is at almost 1500-m altitude and away from heavy industry. The campus is above the valley fog and occasional winter inversion layer, and the campus is at the mouth of a canyon that is the source of clear nighttime winds out of the high mountains. Consequently, the number of nights observed is limited more by resources than by observing conditions.

The location is also good because of the existence of other instrumentation nearby for correlative and validation studies. ALO is part of the USU cluster of mesospheric instruments. The other part of the cluster is the Bear Lake Observatory (BLO), located 38 km away in a dark and electromagnetically quiet location. Since its inception in 1990, BLO has been home from time-to-time for several instruments capable of making mesospheric observations. These have included a very sensitive Fabry-Perot interferometer for OH winds and temperatures from approximately 87 km[20–22], all-sky cameras to observe OH, O_2, and O(^{1}S) emissions[23], instruments to measure rotational temperatures from OH or O_2[24], and a digital ionosonde that can also operate in meteor and IDI modes[25,26]. In addition to the USU cluster, radiosondes are launched at 0000 and 1200 UT from five locations within 400 km of ALO: Salt Lake City, UT; Boise, ID; Lander, WY; Grand Junction, CO; and Ely, NV.

The ALO location is also good for studying several aspect of the generation, propagation and breaking of gravity waves. Northern Utah is located within one of the more mountainous regions of the world, which stretches from almost the Pacific coast in the west to the Great Plains in the east. This Rocky Mountain region is a major orographic source of gravity waves[9,10] that some believe have a major impact on the mesosphere. In winter the jet stream, another major source of gravity waves[13,14], often passes nearby. The mid-latitude location puts ALO under the average location of the mesospheric jet[27], which is expected to have a major role in filtering upward propagating gravity waves and the structure of which arises from gravity wave breaking. In addition, the location is under the middle of the latitude region where mesospheric inversion layers occur[28]. While these inversions are not fully understood, they are believed by many to be closely related to upwardly propagating gravity waves[29–32].

3. CURRENT RAYLEIGH-SCATTER LIDAR SYSTEM

3.1 Rayleigh-scatter lidar

The current lidar system is a vertically pointing, coaxial system. It consists of a frequency-doubled Nd:YAG laser (Spectra Physics GCR-5, Table 1), a 44-cm diameter Newtonian telescope, a cooled photomultiplier tube (PMT) housing (Products for Research), and a red-sensitive bialkali PMT (Electron Tubes 9954B). The intense low-altitude returns are (partially) blocked by a rotating chopper (Oriel), which is fully open at approximately 18 km, and by an electronic gate (Products for Research) for the PMT. The latter changes the gain by almost 10^3 and is gated on at 38 km, providing good data from below 45 km to above 90 km. The pulses from the PMT are amplified by 200 and sent to a multi-channel scaler with built-in discriminator (EG&G Turbo MCS). The gate width is 250 ns (37.5 m) and 14000 gates (525 km) are sampled. The samples are accumulated for 2 minutes, or 3600 laser shots.

Table 1. ALO laser for Rayleigh scatter

Spectra Physics GCR-5	
Wavelength	532 nm
Energy per Pulse	600 mJ
Pulse-Repetition Rate	30 Hz
Power	18 W @ 30 Hz
Pulse Length	7 ns
Spectral Width (Seeded)	< 150 MHz
Beam Divergence	< 500 μrad

While the power of a laser is usually given as average power, 18 W in this case at 532 nm, it can also be given as peak power, which is 2.6 GW. This system typically produces 360 counts from 45 km in one gate after 2 minutes, which is equivalent to 4.0×10^5 counts/s. In the present configuration, the PMT starts to become nonlinear at 2–3 times this count rate. Consequently, with one detector, 45 km is taken to be the lowest good altitude. While some light does get around the

chopper, enough to clearly identify clouds, the peak levels are less than the signal at 39 km, right after the electronic gate turns on. The number of gates, or maximum range, is large to provide a diagnostic of the PMT behavior. When the peak signal level is not too high and the electronic gate is working properly, the background level should be constant. If it increases, decreases, oscillates, or has a bump, something needs to be corrected. Lastly, the telescope field of view is approximately three times the beam divergence or 1.5 mrad.

The ALO Rayleigh lidar system is compared to several others in Table 2. The figure of merit is the power-aperture product, the product of the laser power and the unobstructed area of the receiving telescope, given in W-m^2. It works well so long as all the lidars operate at the same wavelength and nothing happens to either the emitted laser beam or the backscattered signal. Less quantifiable factors such as greater atmospheric transmission (as at ALO and MLO), more sensitive PMTs, and better system efficiencies are not included. While having a small figure of merit, ALO is well within the range of these other lidars. Its small telescope is largely compensated for by the laser, which has been tuned for maximum power.

Table 2. Comparison of Rayleigh-scatter lidars

Lidar	ALO	OHP[33,34]	CEL[33]	Fukuoka[35]	Wales[36]	York/ISTS[37]	MLO[34]
Emission λ (nm)	532 nm	532 nm	532 nm	353 nm	532 nm	532 nm	353 nm
Energy (mJ)	600	400 (300)	200	200	500	500	50
Pulses / sec (Hz)	30	15 (50)	30	80	15	20	200
Power (W)	18	6 (17.5)	6	16	7.5	10	10
Aperture Dia. (m)	0.44	0.8 (1.0)	1.2	0.50	0.90	0.50	1.0
Correction Factor	1.0	1.0 (1.0)	1.0	1.0[a]	1.0	1.0	1.0[a]
Fig. of Merit (W-m^2)	2.7	3.0 (13)	6.7	3.1	4.8	1.9	7.8

[a]Assumed that the greater scattering at 353 nm is offset by greater absorption in the atmosphere and system.

3.2 Data reduction

The procedure used to determine temperatures and uncertainties from the observations is described in Wickwar et al.[38]. In essence, it involves at initial temperature at the highest altitude, which is where the signal is 16 times as big as the standard deviation, and a downward integration. The numerical integration has been carefully checked and the basic procedure verified with a simple simulation of the lidar data.

The reduction procedure to obtain temperatures has been and continues to be very carefully examined to minimize systematic errors. This requires careful determination of the background signal and checking for PMT saturation at low altitudes. It requires examining each 2-minute integration. It has involved determining the altitude of the laser, the value of *g* at the laser, and the effect of an altitude-varying mean molecular weight. A full simulation of the data is also currently underway to better understand the derived temperature at the highest altitudes. Because the observations were initially aimed at finding the temperature climatology and were acquired at night at mid latitudes, the initial values used in the integration were taken from the nighttime climatology[39] from resonance-scatter lidar observations at Ft. Collins, Colorado. In that way, our climatological temperatures should be valid to a higher altitude than if we had used initial values from another source. They should also be valid to a higher altitude than temperatures derived for shorter time scales because the latter might be influenced by planetary waves or large-scale gravity waves.

Another way to assess the validity of the observation and data-reduction procedure is to compare the temperatures to those obtained by other Rayleigh lidar groups at similar latitudes and to those obtained by different techniques. Such comparisons have been carried out with several sets of data[40,41]. In general, good agreement has been obtained among the temperature profiles. However, some differences, localized in time and altitude, were found. Because of the overall good agreement, these differences may well reflect significant geophysical differences that warrant further investigation.

3.3 Database

Between August 1993 and the present an extensive database has been acquired. Table 3 gives a summary of the hours and nights observed. The variations reflect many different things including equipment problems and changes, funding, and operating procedures. While weather has affected the number of nights observed in a few months, it has not been a major impediment. With this extensive database, the data can be examined on

Table 3. Hours and Nights Observed

Dates	*Hours*	*Nights*
Aug. 93 – Jul. 94	375	56
Aug. 94 – Jul. 95	649	95
Aug. 95 – Jul. 96	372	59
Aug. 96 – Mar. 97	560	72
May 98 – May 99	553	93
June 99 – Apr. 00	745	134
Totals	*3,254*	*509*

many different time scales.

The influence of the initial value is minimal after 20 km and may be small after only 5 or 10 km for a climatological average. However, as the altitude of the initial point increases, the importance of a well-behaved background becomes greater and the need to consider variations in the proportion of neutral constituents increases. Nonetheless, the greater initial altitude leads to a higher altitude at which the temperatures are good. In addition, the uncertainty at a given altitude decreases.

4. MESOSPHERIC TEMPERATURES

4.1 Sampling the results

Turning first to Figure 1, it shows the temperature climatology at ALO for the period 1994 though 1999. Each curve is for a different month, with the three dotted curves for summer (May–July), the three dashed curves for winter (December–February), and the solid curves for the two equinox periods. These curves were obtained by averaging all the one-hour temperatures within a given month for all years. The top altitude is reached when the number of curves contributing to this average falls to half the number at the lowest altitudes. The altitude resolution is 3 km. Near the stratopause, the temperature clearly responds to solar heating, being 10% hotter in summer than in winter. However, above 60–65 km the situation changes and the winter temperatures become significantly warmer than the summer temperatures. For some months this change in behavior occurs gradually with altitude, while for some of the winter months it is very abrupt. This temperature behavior in the upper mesosphere is caused by dynamics, as discussed in the Section 1.

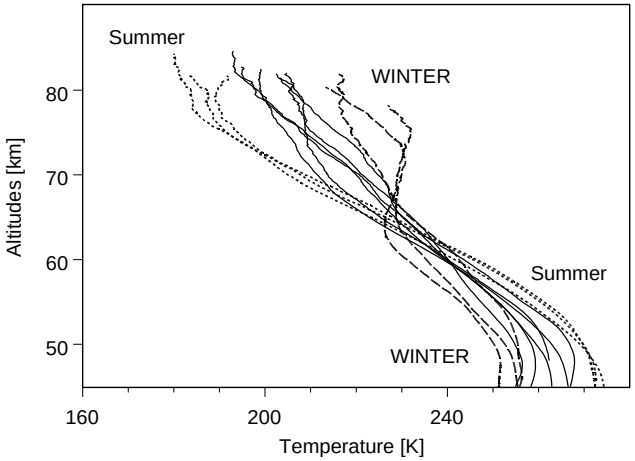

Figure 1. Monthly mean temperature profiles above ALO. The summer months are May–July, the winter months December–February. The data are from 1994–1999.

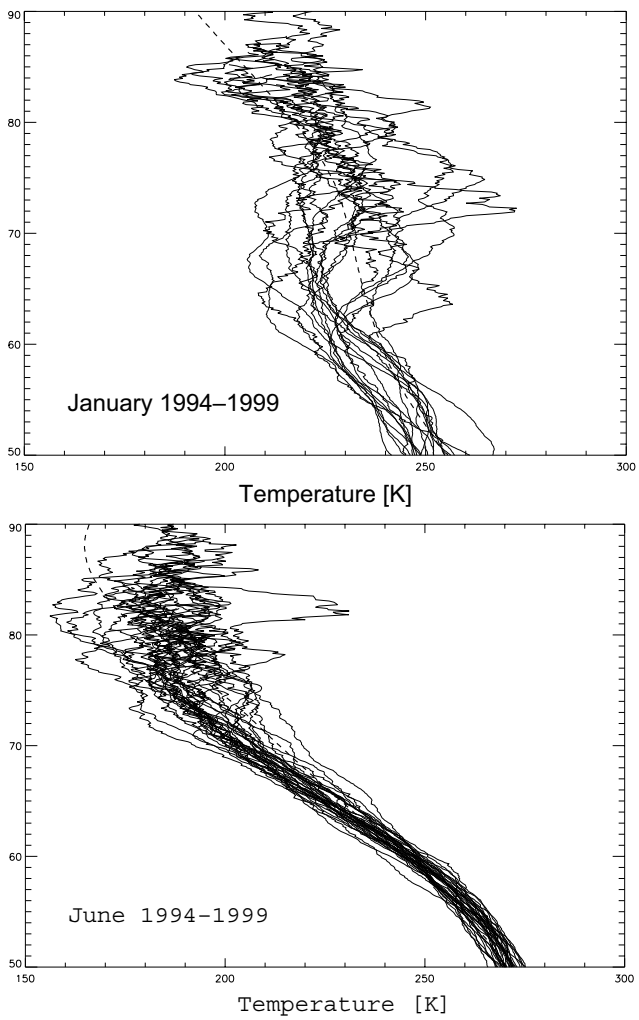

Figure 2. Comparison of winter and summer mesospheric temperatures. The ordinate is altitude in km. (See text.)

More insight into the behavior can be obtained by looking at the average nightly profiles that go into the long-term average in Figure 1. The curves for January and June are shown in Figure 2, along with the corresponding curves from the MSISe90 empirical model[42]. To the extent that they can be seen, these latter curves are a useful reference. As in Figure 1, the altitude resolution is 3.0 km. In the winter profiles, the most striking feature is the occurrence of large oscillations above 60 km. This is the mesospheric inversion layer[43,44,30]. Our data show minimum-to-maximum amplitudes that can approach 50 K. When examined with even finer time resolution, with 1-hour averages, many of the inversion-layer curves show a downward phase velocity and a vertical wavelength such that they appear to be closely linked to the diurnal tide. A period with 10 nights of observations during an 11-day period in late February 1995 was examined by Meriwether et al.[32] and compared to model predictions from the Global-Scale Wind Model (GSWM)[62]. While this supports the tie to the tide, the observed amplitudes are approximately an order of magnitude greater than can be accounted for by the model. This discrepancy is similar to, but even larger than the one between the amplitude of the 12-hour tidal winds deduced from Fabry-Perot observations of OH winds at BLO at 87 km in late summer and those modeled with the GSWM. In other

periods a consistent behavior, judged by the peak altitude, will occur for several days and then change. Similarly, the behavior in data from different years can appear very different[45]. It is not clear at this time what produces these changes in behavior

The bottom part of Figure 2 shows the June temperature profiles. In addition to the warmer stratopause and colder upper mesosphere, these curves show a more consistent behavior from night-to-night than the winter data. Very little spread in the values occurs below 70 km, and above that altitude it is significantly less than in winter. Explanations for these differences largely involve seasonal changes in wave filtering by the mesospheric jets, which reverse direction from winter to summer.

Another way to look at the temperature structure is to examine contour plots. The top plot in Figure 3 is from the same ALO data as in Figure 1. The bottom plot, from the MSISe90 empirical model[42], is for comparison. While, overall, considerable similarity exists, some major differences are readily apparent. The biggest difference is in the winter behavior in January and February. Even with the multi-year averaging, the ALO data shows much stronger effects from the wintertime intermediate layers. Throughout the year, the upper mesosphere temperatures are 10–30 K warmer than in the model. In the lower mesosphere, the summer maximum in temperature occurs at least a month earlier than in the model. Some of these differences are examined elsewhere[38,41]. These papers also show an intriguing difference between the Rayleigh and sodium resonance temperatures in the limited altitude region where they overlap.

In addition to direct temperature observations, we have another observation that indirectly suggests lower temperatures than we have measured in the summertime mid-latitude upper mesosphere. On the evening of 22 June 1999 local time (23 June 1999 UT), a noctilucent cloud (NLC) was observed visually from Logan, UT, and the following evening it was observed overhead with the lidar[46]. A convenient way to display the lidar return is as the backscatter ratio R, the ratio of the observed signal to what it would have been from Rayleigh scatter alone. This is done in Figure 4 for Δh=337.5 m and Δt=12 minutes, starting at 04:22 on 24 June 1999 UT between 80 and 84 km as solid lines with 1-standard deviation error bars. The abscissa applies to the first profile, the left-most one, and each of the four successive profiles is shifted to the right by R=2. Each profile is shown along with a dashed reference line obtained with Δt=1 hour starting at 04:22 UT. A comparison of these pairs of profiles shows a layer changing in strength and altitude. The major characteristics of the NLC were a peak altitude between 81.6 and 82.4 km, a thickness that varied between 400 and 800 m, a rate of descent of 24 cm/s, and a maximum backscatter ratio of 4.7 at 82.4 km. Other measures of the maximum strength of the backscattered signal are a volume-backscatter coefficient of

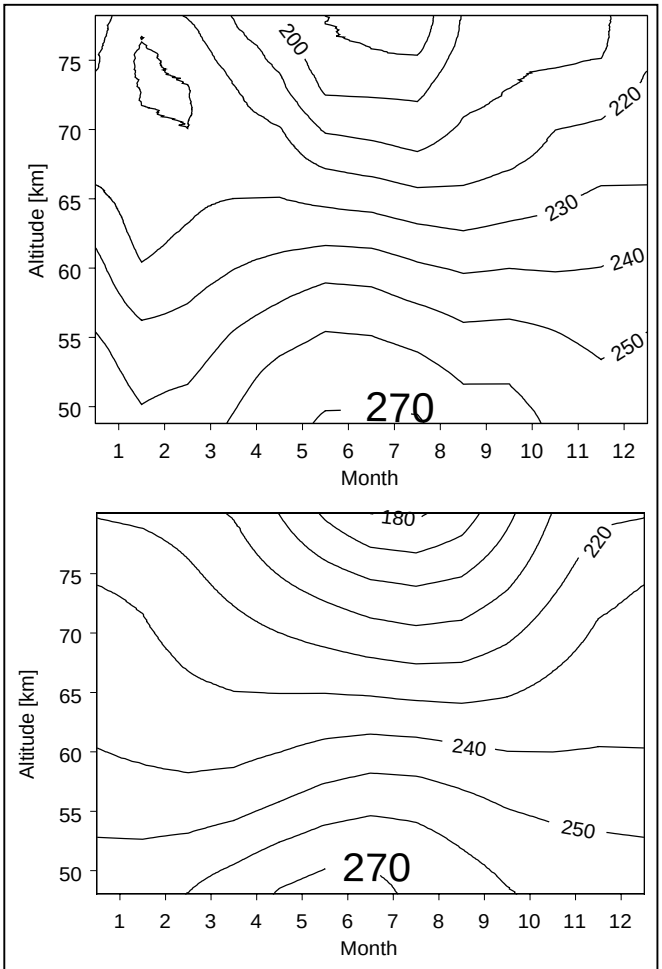

Figure 3. Temperature climatology above ALO from 1994–1999 observations (Top) compared to the MSISe90 model (Bottom).

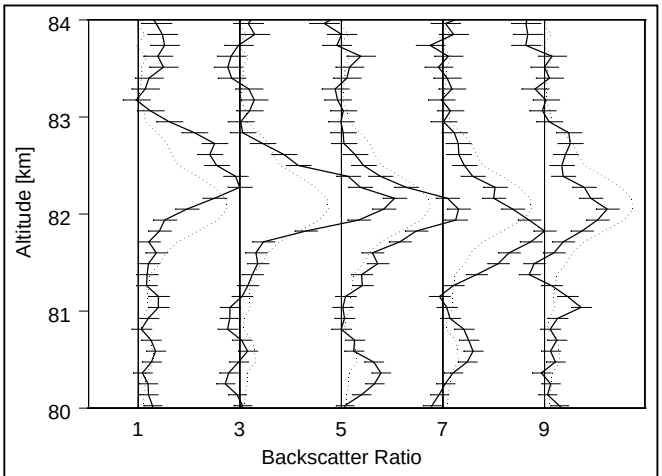

Figure 4. Backscatter ratios for the NLC seen from ALO between 10:22 and 11:22 PM (MDT) on 23 June 1999 (MDT). Each successive 12-minute curve is shifted to the right by 2 units in backscatter ratio.

1.6×10^{-10} m^{-1}-sr^{-1} and a range-corrected equivalent Rayleigh altitude of 76 km. This was a very weak and thin NLC, which would be consistent with the equatorward edge of a NLC.

Past observations and reviews of noctilucent clouds[47] and polar mesospheric clouds[48] indicate that they are a polar phenomenon with an equatorward boundary at approximately 50°N. This visual detection at 41.7°N is approximately 8° equatorward of this boundary and the lidar detection is 11° equatorward of the lowest latitude previous lidar detection at 52.4°N in Wales[49]. Thus, NLCs have graduated to also being a mid-latitude phenomenon. This detection could be a significant indicator of global change. It could occur because of an increase in greenhouse gases that cool the mesosphere, an increase in methane that would lead to more water vapor in the upper mesosphere, or a combination of the two[50]. Less directly, it could also arise because of an increase in the meridional circulation, perhaps as a result of an increased generation of gravity waves, leading to greater adiabatic cooling in the summer hemisphere (and warming in the winter hemisphere) or because of a significant temperature oscillation with a minimum at 82 km that lowers the usual local temperature. In either case, this unexpected (at least at this time) observation requires the extension of future coordinated NLC observations to mid and lower latitudes. These observations need to be comprehensive enough to distinguish among possible causes.

4.2 Projects underway

As noted in Section 1, because of ALO's location in the middle of the Rocky Mountain chain, the possibility exists for finding significant longitudinal differences in temperature. The extent of these rugged mountains in western North America, make them one of the most significant orographic sources in the world. Some of these waves are seen at low altitude in the lidar data as they pass through cirrus clouds, Figure 5. The data shown are for 2-minute intervals and 112.5-m altitude resolution. Apparent in the figure is a downward phase progression, the vertical wavelength (just over 1 km), and the apparent period (approximately 30 minutes). However, it remains to be shown whether these gravity waves have a significant impact on mesospheric structure. A counter argument to the orographic source is that mesospheric effects depend more on gravity wave filtering than on the sources. Nonetheless, some early results from ALO and BLO, suggest possible effects. For instance, in winter, the stratopause temperatures were cooler and the upper mesospheric temperatures warmer than the French found[33]. The amplitude of the semidiurnal tide (or at least of a 12-hour oscillation) in the OH winds at 87 km observed with a Fabry-Perot interferometer in December and January at BLO was less (i.e., undetectable) than seen elsewhere with MF radars[51]. While these might be real longitudinal differences, they might also be the result of comparing limited amounts of ALO and BLO data with much longer time sequences for other data.

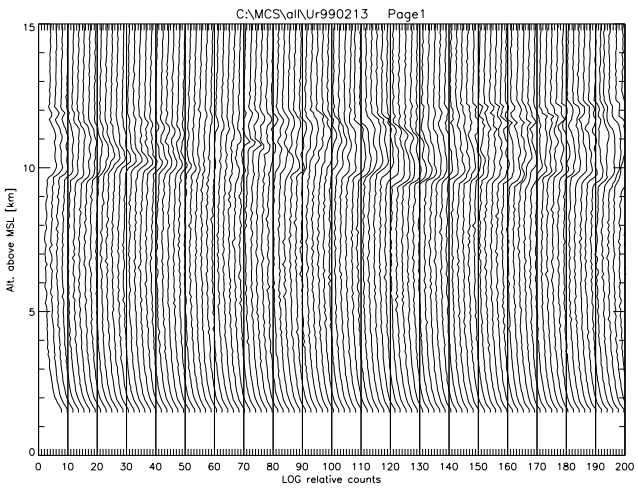

Figure 5. Gravity waves in cirrus clouds during 3 hours and 20 minutes on 13 February 1999. The ordinate is altitude in km; the abscissa is labeled in minutes. Mie scatter occurs from cirrus clouds between 10 and 12 km. Each 2-minute profile is shown as the log of the count rate.

Accordingly, one of the projects underway is to compare the ALO temperatures with those from other climatologies at similar latitudes. The intent is to look for significant differences that cannot be accounted for by data reduction procedures or data selection. This effort commenced with the visit of a USU student to the University of Western Ontario, which operates the Purple Crow lidar[51], at the beginning of the summer. This lidar is at almost the same latitude, but is in an extremely flat region. Good overlap exists between the two data sets: the analysis is underway. However, because of filtering arguments, a comparison with one site is not sufficient to make the case for longitudinal differences. Hence, we are constantly on the lookout for other data sets with which to compare.

Another approach to these comparisons is to compare the observations to calculations with general circulation models that include gravity wave parameterization and filtering. If temperature differences are found between two sites, such a comparison may help to distinguish between a gravity wave source and filtering. More generally, if the gravity wave sources in the model have been tuned to reproduce a different type of observation, or an observation at a different latitude, the comparison will provide information on whether these same sources will also reproduce the mesospheric temperatures observed with the lidar. Agreement would be significant, but differences might provide information on the gravity wave parameterization or on the assumed saturation mechanism, e.g., linear, Doppler spread, diffusive. Depending on the

differences, they may also provide information on other inputs to the model. We have initiated a comparison with the TIME-GCM[53,54]. Enough significant differences exist in general circulation models that we are also interested in comparing with other models.

While gravity waves may have a big impact on the temperature structure, information about them can be obtained more directly by examining the variability of both the density and temperature data[35,36,55–58]. Initial studies have been performed with ALO data[59,60]. This approach is being continued with the more extensive database that now exists. Currently, we are working with Robert Sears in examining the densities for variability on nightly, monthly, seasonal, and annual scales. This should help characterize the climatology of the gravity waves that reach the mesosphere and to which the lidar is sensitive. We hope to extend this work to develop a climatology of density variance, horizontal and temporal correlation lengths, profiles of power-spectral density slopes, and profiles of the deposition of turbulent energy as a function of period and wavelength.

Table 4. ALO Large Lidar Telescope

Each Mirror	
Dia. of Primary	1.27 m
Dia. of Secondary	0.36 m
Effective Area	1.16 m^2
Primary f.l.	2.41 m
Effective f.l.	10.2 m
Blur Circle	0.3 mm
Max. FOV	5 mrad
Four-Barrel Telescope	
Total Eff. Area	4.66 m^2
Azimuth ∠ Range	0°–360°
Zenith ∠ Range	0°–45°

In examining the strong mesospheric inversion layers in winter, one of the striking features is that they can be very similar for several days, as in the period discussed by Meriwether et al.[32], and then change rapidly. Assuming that the inversion layers are closely related to gravity-wave activity, this change suggests that the gravity-wave source (or the filtering mechanism) has changed. To test this, we will compare days with different temperature structures to potential gravity wave sources, i.e., to winds over the mountains, to the location and strength of the jet stream, and to frontal activity. If, for instance, a distinct pattern or correlation is established with winds over the mountains instead of with jet-stream activity, that will be interesting in itself and will also support the notion that longitudinal variations should exist.

In the above discussions of the temperature structure, the interest has been on variations over the course of weeks, months, and years. The inputs are nightly averaged temperatures. However, the lidar database is extensive enough to allow, with the appropriate averaging, a search for temporal variations on the scale of hours, i.e., for tides. An initial attempt to do so[61], using one-hour bins, was reasonably successful. Oscillations were found with what appeared to be six, eight, and twelve hour periods. Some grew with altitude. In addition, the winter inversion layer has been associated with the 24-hour tide[32]. The expanded database will make it much easier to look for tide-like variations. Although, as always, questions will arise because the database is only comprised of nighttime data. To help sort out the oscillations, they will be carefully compared to the Global-Scale Wind Model (GSWM)[62].

5. FUTURE DIRECTIONS

5.1 Large Lidar Telescope

The observations discussed and shown in Section 4 have all been made with the 44-cm Newtonian telescope described in Section 3. To improve future observations, a much larger telescope is under development. To obtain a large collecting area at minimal cost, the design is unusual. It is consists of four co-aligned telescopes with a total collecting area equivalent to that of a 2.5-m telescope, i.e., 5.0 m^2. More specific information is given in Table 4. The azimuth-elevation mount is shown in Figure 6, fixed for now in the zenith position, with one primary-secondary pair of mirrors installed. The other three primary-secondary pairs of mirrors have been made, ground, and polished. When tests are

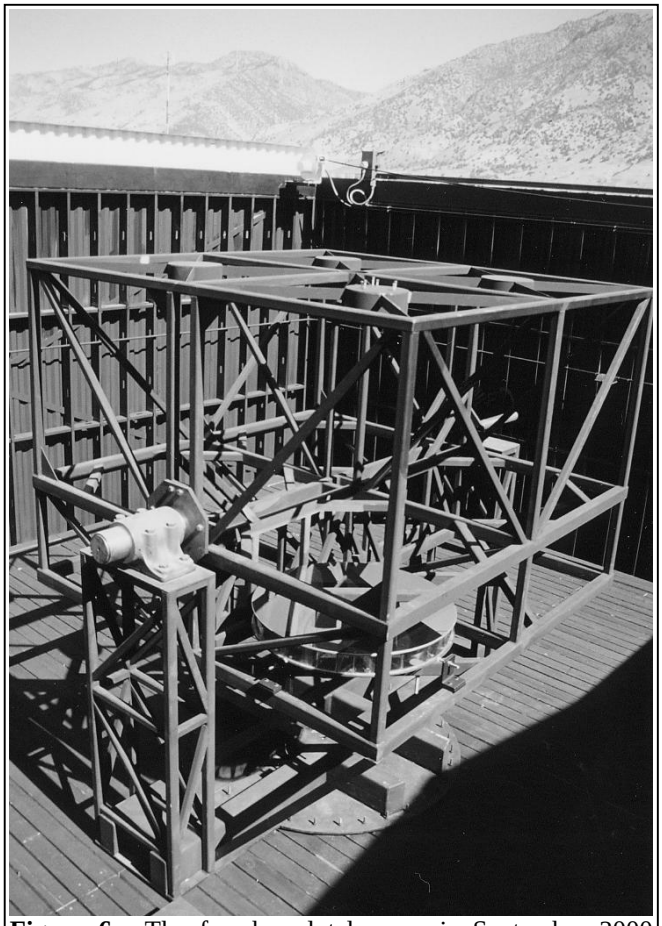

Figure 6. The four-barrel telescope in September 2000 with the first 1.25-m primary and matched secondary.

completed on the first pair, they will have their final polishing, testing, and coating and then they will be installed. To house the telescope, a large observatory building was built, which is shown in Figure 7 with the roof open. The observatory was sized to enable the telescope to point in any direction up to 45° off zenith.

Figure 7. The lidar observatory in August 2000 with the roof open. The building is approximately 10 m×10 m×7 m.

The collecting area of the large lidar telescope is 33 times that of the current telescope. Taking into account blockage by the secondaries, the figure of merit for the Rayleigh lidar will increase from 2.7 to 84 W-m^2. This will greatly increase the Rayleigh-scatter capability. The greater sensitivity can be used to reduce the integration time, to increase the maximum altitude, to improve the measurement uncertainty, or various combinations of these depending on the research requirements. In one scenario, the integration time would be reduced to 15 minutes, approximately the shortest time consistent with hydrostatic equilibrium. These profiles would have the same precision as those now obtained in an 8-hour night. Alternatively, the precision for these profiles would be 2.8 times better at every altitude than obtained now in a 1-hour integration. Or, the precision of these profiles at high altitudes would be equivalent to what can now be obtained in a 1-hour integration at a 13-km lower altitude. In a second scenario, the integration times would be unchanged. The precision at the same altitudes would improve by a factor of 5.6. Or, the precision of these profiles at higher altitudes would be equivalent to what can now be obtained at a 21-km lower altitude. Ignoring potential difficulties (and opportunities) from changes in neutral composition, this would enable temperature measurements to 105 or 110 km. The upgraded ALO Rayleigh lidar is compared in Table 5 to several others in this new category of large lidars.

Table 5. Comparison of large Rayleigh-scatter lidars

Lidar	ALO	ALOMAR[63]	Firepond	PCL[52]
Emission λ (nm)	532 nm	532 nm	532	532 nm
Energy (mJ)	600	30	700	60
Pulses / sec (Hz)	30	30	30	20
Power (W)	18	11	21	12
Aperture Dia. (m)	2.5	1.8	1.2	2.6
Correction Factor	1.0	0.50[a]	1.0	1.0
Fig. of Merit (W-m^2)	84	14	24	66

[a]Half the light goes to the normal Rayleigh channel; half goes to the DWTS.

5.2 Resonance Capability

Additional information on what is happening in the transition region from the upper mesosphere to the lower thermosphere can be obtained by adding a resonance-scatter capability. For that purpose, ALO acquired an alexandrite ring laser (Light Age, Inc.). This is the same laser as two that the Institute for Atmospheric Physics (IAP) at Kühlungsborn, Germany, acquired and used very successfully to determine temperatures and potassium densities from potassium resonance scatter[64–66]. This approach to resonance scatter has the simplifying advantage of being based on a solid-state laser and an external-cavity diode laser for seeding. To determine temperature, the laser has to be scanned over the potassium spectrum. An absolute wavelength reference will be determined by observing the Doppler-free potassium spectrum. The scanning will be performed by locking the seed laser (Newport/EOSI) to a computer-controlled capacitance-stabilized etalon (CSE) (Hovemere, Ltd.). The etalon gap will be varied to locate the Doppler-free reference line and then will be stepped across the potassium spectrum. The seeder lockbox will adjust the seeder wavelength to maximize the signal from the emission passing through the CSE, thereby locking the seeder and the alexandrite to the etalon. With this approach, the number of wavelengths included in the stepped scan across the potassium spectrum can be varied from, for instance, two to 20. This will provide flexibility to make detailed measurements of the spectrum to insure that the equipment is working as expected or to make measurements at just two or three spectral positions to make high time resolution measurements for temperature (and wind) determinations. A high-resolution Fabry-Perot interferometer (Hovemere, Ltd.) will also be used as a laser spectrum analyzer (LSA) to examine each outgoing laser pulse for wavelength, spectral width, and power. If the laser pulse is good, the sampled data will be added to the accumulated signal. Otherwise, the data will be discarded. Beyond this, the pulse repetition rate of the laser will be increased from 25 to 30 Hz to interleave them with the Nd:YAG pulses to

Table 6. ALO laser for Resonance scatter

Light Age, Inc., alexandrite ring laser	
Wavelength	770 nm
Energy per Pulse	~ 150 mJ
Pulse-Repetition Rate	30 Hz
Power	4.5 W @ 30 Hz
Pulse Length	160 ns
Spectral Width (Seeded)	~ 20 MHz
Beam Divergence	< 1.0 mrad
CSE (free-spectral range)	10 GHz
Number of steps	1024
LSA (free-spectral range)	1 GHz
Finesse	50

obtain simultaneous Rayleigh and resonance observations. Many of the characteristics of this system are given in Table 6. During the last year considerable experience has been acquired in the laboratory with operating the alexandrite laser and controlling its wavelength. This experience has been gained making O_2 and H_2O absorption measurements. The O_2 observations can be made directly with the laser; the H_2O observations require Raman shifting the laser beam in H_2 to obtain the correct wavelength. An example of H_2O absorption for 6, 16, and 56-m path lengths is given in the bottom part of Figure 8. The alexandrite wavelength was referenced to a known O_2 rotational line near 766.8 nm, near the center of the alexandrite tuning range. The spectrum was then scanned by varying the seeder wavelength. The spectral purity of the alexandrite laser was monitored with the LSA. The Raman-shifted laser output was scanned over the H_2O features near 1125.4 nm in steps of 1.5 GHz. Each scan took 15 minutes. The top part of Figure 8 shows model calculations of the H_2O absorption for the three path lengths. The modeling used a Voigt profile function with line positions from the 1996 HITRAN database. The H_2O column densities were based on 1500-m elevation and a mid-latitude atmosphere at 30% relative humidity (the measured value). The experience gained from this work will be very valuable preparation for making our first potassium observations.

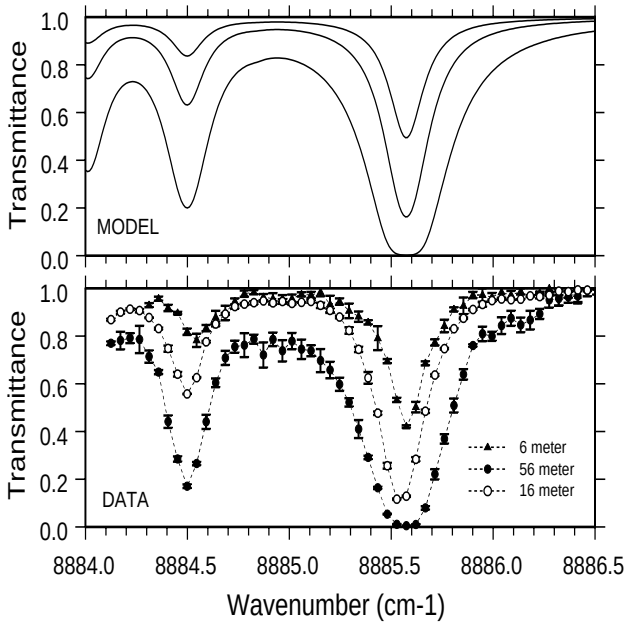

Figure 8. The absorption spectrum and model calculations for two H_2O lines near 1125.4 nm. (See text.)

An important question concerning these potassium observations is how they will compare to those by the IAP group and how they will compare to the sodium observations made elsewhere. An indication can be obtained by extending the figure of merit discussed in Section 3.1. A complication arises for resonance scatter in that a change in wavelength means a change in scattering constituent, i.e., from potassium to sodium. This implies that the relative densities and cross sections have to be introduced into the figure-of-merit calculations. The results are given in Table 7 referenced to a sodium lidar.

Table 7. Comparison of Resonance-scatter lidars

Lidar	ALO	IAP[64,66]	Ft.Collins[a]	Urbana[67,68]	ALOMAR[b]	PCL[69]
Emission & λ (nm)	K at 770	K at 770	Na at 589	Na at 589	Na at 589	Na at 589
Energy (mJ)	150	100	30	30	30	60
Pulses / sec (Hz)	30	25	50	20	30	20
Power (W)	4.5	2.5	1.5	0.60	0.90	1.2
Aperture Dia. (m)	2.5	0.80	0.36	1.0	1.8	2.6
Correction Factor	0.011[c]	0.011[c]	0.50[d]	1.0	0.50[d]	1.0
Fig. of Merit (W-m^2)	0.23	0.014	0.074	0.47	1.1	6.6

[a]Based on memory of upgraded system seen in June 2000. [b]Estimated.
[c]Based on the ratios of peak number densities[66,70] and scattering cross sections[71,72], i.e.,
$[N_{MAX}(K) / N_{MAX}(Na)] \times [\sigma(K) / \sigma(Na)] = [5.0\times10^{7} / 4.0\times10^{9}] \times [1.34\times10^{-15} / 1.52\times10^{-15}] = 1.10\times10^{-2}$.
[d]The output is split between two telescopes.

A comparison of the alexandrite-based resonance lidars at ALO and IAP shows that with the four-barrel telescope at ALO the figure of merit is 16 times bigger at ALO than at IAP. (If the 44-cm telescope were used at ALO, then the ratio would be 0.5.) Everything else being equal, this implies that similar temperature results could be obtained in 1/16th the time at ALO as at IAP, e.g., 4 minutes instead of 1 hour. Alternatively, with the same asssumption, this implies that for the same integration times, the uncertainty at ALO would be 1/4th of what it would be at IAP. Either way of comparing these systems implies that good potassium temperatures will be obtained with the system at ALO. Moreover, they can be obtained with shorter integration times than for the ALO Rayleigh lidar.

Turning to the sodium systems, it is apparent that the big advantage to observing sodium is its much greater density. However, the large collecting area of the four-barrel telescope largely overcomes this advantage. The ALO figure of merit is larger than for the lidar at Ft. Collins and smaller than for the University of Illinois lidar at Urbana. Based on what has been accomplished with these two lidars, this again implies that ALO will be able to obtain good temperatures. The comparison with Illinois also indicates that ALO would be able to obtain good winds. However, the comparisons with ALOMAR and PCL, both with large telescopes, indicate they are significantly more sensitive.

The addition of the resonance capability to ALO will greatly improve the ability to measure temperatures in the transition region from the mesosphere to the lower thermosphere, 80–105 km. The resonance lidar will be able to do this directly and it will be able to improve the Rayleigh observations in this region by providing the initial temperature for the data reduction. In contrast, the Rayleigh system will provide the continuous observations from the stratosphere to this transition region. In the overlap region above 80 km, the Rayleigh system will be sensitive enough to provide good comparisons between the two very different types of temperature measurements. Questions will arise concerning Rayleigh scatter and a changing mean molecular mass, e.g., the ratio of atomic-to-molecular oxygen densities. Initial observations at PLC[69] have already raised questions about the effect of variations in the ratio of N_2 to O_2. There should be much to learn by having simultaneous observations with these two techniques at the same location. Additional correlative temperatures could be obtained, as discussed in Section 2, from instruments at BLO. Furthermore, the possibility exists to add a wind capability, Section 5.4.

5.3 New data-acquisition system

To take advantage of the greater Rayleigh signal from the four-barrel telescope and the resonance signal from the alexandrite laser, a multi-channel data-acquisition system with some additional features is needed. A four-channel system is currently being built by Hovemere, Ltd. Particulars are given in Table 8. It is designed for four channels, but will initially be used for three: two will be devoted to Rayleigh scatter to cover the extended altitude range and one, with a GaAs photomultiplier tube, will be devoted to resonance scatter. It differs from the current system in that it accumulates the photon counts from all the gates in the computer instead of in the photon-counting hardware. This provides greater flexibility without taxing today's PCs. For resonance scatter, this system will allow every pulse to be examined with the LSA for wavelength, spectral width, and power so that a decision can be made to reject or accept and accumulate the data. For both lidars it enables other data such as laser power, pointing directions, etc. to also be collected and recorded. The overall system will be controlled by LabVIEW.

Table 8. New data-acquisition system

Number of channels	4
Number of gates / channel	5000
Gate width (0.667 μs)	100 m
Discriminators	Internal
Summation	In the PC

5.4 Spatial structure and winds

Although currently pointing in the zenith, the telescope and observatory building were built, as mentioned in Section 5.1, to point anywhere up to 45° off zenith. The intent is to add the motors to point the telescope, the mirrors to direct the laser beams, and the controls to keep the laser beams and telescope co-aligned. This will open the way to observations of the spatial structure of densities and temperatures and to observations of winds. Spatial structures could be observed with both the Rayleigh and resonance lidars. Winds could be observed with the resonance lidar because the setup (controls) for winds is the same as for temperatures. Rayleigh winds, however, would require a new detector system such as the Doppler Wind and Temperature System at ALOMAR[73,63].

6. ACKNOWLEDGEMENTS

This research was supported in part by NSF CEDAR grant ATM9714789 and by the US Army Research Office for R&D support on IR water-vapor line shapes. Lidar observations under this grant were carried out by a dedicated group of students. In addition to coauthor Joshua Herron, this group includes Brian Anderson, Joel Drake, Will Fredin, Bethany Martineau, Karen Marchant Nelson, Patrick Neary, and Marie Westbrook.

7. REFERENCES

1. R.J. Murgatoyd, "Winds and temperatures between 20 km and 100 km—A review", Quart. J. Roy. Meteor. Soc. 83, pp. 417–458, 1957.
2. C.B. Leovy, "Simple models of thermally driven mesospheric circulation", *J. Atmos. Sci. 21*, pp. 327–341, 1964.
3. M.R. Schoeberl and D.F. Strobel, "The zonally averaged circulation of the middle atmosphere", *J. Atmos. Sci. 35*, pp. 577–591, 1978.
4. J.R. Holton and W.M. Wehrbein, "A numerical model of the zonal mean circulation of the middle atmosphere", *Pageoph. 118*, pp. 284–306, 1980.
5. M.A. Geller, "Dynamics of the middle atmosphere", *Space Sci. Rev. 34*, pp. 359–375, 1983.

6. R.R. Garcia and S. Solomon, "A numerical model of the zonally averaged dynamical and chemical structure of the middle atmosphere", *J. Geophys. Res. 88*, pp. 1379–1400, 1983.
7. C.O. Hines, "Internal atmospheric gravity waves at ionospheric heights", *Can. J. Phys. 38*, pp. 1441–1481, 1960.
8. R.S. Lindzen, "Thermally driven diurnal tide in the atmosphere", *Quart. J. R. Meteorol. Soc. 93*, pp. 18–42, 1967.
9. G.D. Nastrom and D.C. Fritts, "Sources of mesoscale variability of gravity waves. Part I: Topographic excitation", *J. Atmos. Sci. 49*, pp. 101–110, 1992.
10. J.T. Bacmeister, "Mountain-wave drag in the stratosphere and mesosphere inferred from observed winds and a simple mountain-wave parameterization scheme", *J. Atmos. Sci. 46*, pp. 377–399, 1993.
11. M.J. Alexander, J.R. Holton and D.R. Durran, "The gravity wave response above deep convection in a squall line simulation", *J. Atmos. Sci. 51*, pp. 2212–2226, 1995.
12. M.J. Alexander, "A simulated spectrum of convectively generated gravity waves: Propagation from the tropopause to the mesopause and effects on the middle atmosphere", *J. Geophys. Res. 101*, pp. 1571–1588, 1996.
13. D.C. Fritts and G.D. Nastron, "Sources of mesoscale variability of gravity waves. Part II: Frontal, convective, and jet stream excitation", *J. Atmos. Sci. 49*, pp. 111–127, 1992.
14. T. Tsuda, Y. Murayama, T. Nakamura, R.A. Vincent, A.H. Manson, C.E. Meek and R.L. Wilson, "Variations of the gravity wave characteristics with height, season and latitude revealed by comparative observations", *J. Atmos. Terr. Phys. 56*, pp. 555–568, 1994.
15. R.S. Lindzen, "Turbulences and stress owing to gravity wave and tidal breakdown", *J. Geophys. Res. 86*, pp. 9707–9714, 1981.
16. J.R. Holton, "The role of gravity wave induced drag and diffusion in the momentum budget of the mesosphere", *J. Atmos. Sci. 39*, pp. 791–799, 1982.
17. J.R. Holton, "The influence of gravity wave breaking on the general circulation of the middle atmosphere", *J. Atmos. Sci. 40*, pp. 2497–2507, 1983.
18. R.R. Garcia and S. Solomon, "The effect of breaking gravity waves on the dynamics and chemical composition of the mesosphere and lower thermosphere", *J. Geophys. Res. 90*, pp. 3850–3868, 1985.
19. H. Le Texier, S. Solomon and R.R. Garcia, "Seasonal variability of the OH meinel bands", *Planet. Space Sci. 35*, pp. 977–989, 1987.
20. D. Rees, A. Aruliah, T.J. Fuller-Rowell, V.B. Wickwar and R.J. Sica, "Winds in the upper mesosphere at mid-latitude: First results using an imaging Fabry-Perot interferometer", *Geophys. Res. Lett. 17*, pp. 1259–1262, 1990.
21. G.-H. Choi, I.K. Monson, V.B. Wickwar and D. Rees, "Seasonal and diurnal variations of temperature near the mesopause from Fabry-Perot interferometer observations of OH Meinel emissions", *Adv. Space. Res. 21*, pp. (6)847–(846)850, 1997.
22. G.-H. Choi, I.K. Monson, V.B. Wickwar and D. Rees, "Seasonal variations of temperature near the mesopause from Fabry-Perot interferometer observations of OH Meinel emissions", *Adv. Space Res. 21*, pp. (6)843–(846)846, 1997.
23. G.R. Swenson and S.B. Mende, "OH emission and gravity waves (including a breaking wave) in all-sky imagery from Bear Lake, UT", *Geophys. Res. Lett. 21*, pp. 2239–2242, 1994.
24. R.H. Wiens, S.P. Zhang, R.N. Peterson and G.G. Shepherd, "Tides in emission rate and temperature from the O_2 nightglow over Bear Lake Observatory", *Geophys. Res. Lett. 22*, pp. 2637–2640, 1995.
25. L.-C. Tsai, F.T. Berkey and G.S. Stiles, "Derivation and error analysis of echo phase parameters for the dynasonde", *Radio Sci. 32*, pp. 557–566, 1997.
26. F.T. Berkey, C.S. Fish and G.O.L. Jones, "Initial observations of mesospheric winds using IDI radar measurements at the Bear Lake Observatory", *Geophys Res. Lett.*, Accepted, 2000.
27. E.L. Fleming, S. Chandra, M.D. Burrage, W.R. Skinner, P.B. Hays, B.H. Solheim and G.G. Shepherd, "Climatological mean wind observations from the UARS high-resolution Doppler imager and wind imaging interferometer: Comparison with current reference models", *J. Geophys. Res. 101*, pp. 10455–10473, 1996.
28. T. Leblanc, A. Hauchecorne, M.-L. Chanin, C. Rogers, F. Taylor and N. Livesey, "Mesospheric temperature inversions as seen by ISAMS in December 1991", *Geophys Res. Lett. 22*, pp. 1485–1488, 1995.
29. A. Hauchecorne and A. Maillard, "A 2-D dynamical model of mesospheric temperature inversions in winter", *Geophys. Res. Lett. 17*, pp. 2197–2200, 1990.
30. J.A. Whiteway, A.I. Carswell and W.E. Ward, "Mesospheric temperature inversions with overlying nearly adiabatic lapse rate: an indication of a well-mixed turbulent layer", *Geophys. Res. Lett. 22*, pp. 1201–1204, 1995.
31. T. Leblanc and A. Hauchecorne, "Recent observations of mesopheric temperature inversions", *J. Geophys. Res. 102*, pp. 19471–19482, 1997.
32. J.W. Meriwether, X. Gao, V.B. Wickwar, T.D. Wilkerson, K.C. Beissner, S.C. Collins and M.E. Hagan, "Observed coupling of the mesosphere inversion layer to the thermal tidal structure", *Geophys. Res. Lett. 25*, pp. 1479–1482 & 2127, 1998.

33. A. Hauchecorne, M.-L. Chanin and P. Keckhut, "Climatology and trends of the middle atmospheric temperature (33–87 km) as seen by Rayleigh lidar over the south of France", *J. Geophys. Res. 96*, pp. 15297–15309, 1991.
34. T. Leblanc, I.S. McDermid, A. Hauchecorne and P. Keckhut, "Evaluation of optimization of lidar temperature analysis algorithms using simulated data", *J. Geophys. Res. 103*, pp. 6177–6187, 1998.
35. T. Shibata, T. Fukuda and M. Maeda, "Density fluctuations in the middle atmosphere over Fukuoka observed by an XeF Rayleigh lidar", *Geophys. Res. Lett. 13*, pp. 1121–1124, 1986.
36. A.J. McDonald, L. Thomas and D.P. Wareing, "Night-to-night changes in the characteristics of gravity waves at stratospheric and lower-mesospheric heights", *Ann. Geophysicae 16*, pp. 229–237, 1998.
37. J.A. Whiteway, "Lidar observations of thermal structure and gravity wave activity in the middle atmosphere", Ph.D. thesis, York University, North York, Ontario, 1994.
38. V.B. Wickwar, K.C. Beissner, S. Elkington, S.C. Collins, T.D. Wilkerson, J.W. Meriwether and X. Gao, "Mesospheric temperature profiles determined from Rayleigh-scatter lidar observations above Logan, Utah. 1. Instrumentation and Technique", Manuscript, 2000.
39. J.R. Yu and C.Y. She, "Climatology of a midlatitude mesopause region observed by a lidar at Fort Collins, CO (40.6°N, 105°W)", *J. Geophys. Res. 100*, pp. 7441–7452, 1995.
40. M.G. Shepherd, B. Prawirosoehardjo, S. Zhang, B.H. Solheim, G.G. Shepherd, V.B. Wickwar and J.P. Herron, "Retrieval and validation of mesospheric temperatures from WINDII observations", *J. Geophys. Res.*, Submitted, 2000.
41. V.B. Wickwar, K.C. Beissner, S.C. Collins, T.D. Wilkerson and J.W. Meriwether, "Mesospheric temperature profiles determined from Rayleigh-scatter lidar observations above Logan, Utah. 2. Temperature Results and Comparisons", Manuscript, 2000.
42. A.E. Hedin, "Extension of the MSIS thermosphere model into the middle and lower atmosphere", *J. Geophys. Res. 96*, pp. 1159–1172, 1991.
43. F.J. Schmidlin, "Temperature inversions near 75 km", *Geophys. Res. Lett. 3*, pp. 173–176, 1976.
44. A. Hauchecorne, M.-L. Chanin and R. Wilson, "Mesospheric temperature inversion and gravity wave breaking", *Geophys. Res. Lett. 14*, pp. 933–936, 1987.
45. V.B. Wickwar, K.C. Beissner, T.D. Wilkerson, S.C. Collins, J.M. Maloney, J.W. Meriwether, and X. Gao, "Climatology of mesospheric temperature profiles observed with the Consortium Rayleigh-scatter lidar at Logan, Utah", *Advances in Atmospheric Remote Sensing with Lidar*, edited by A. Ansmann, R. Neuber, P. Rairoux, and U. Wandinger, Springer Verlag, Berlin, pp. 557–560, 1997.
46. V.B. Wickwar, M.J. Taylor, J.P. Herron and B.A. Martineau, "Visual and lidar observations of noctilucent clouds above Logan, Utah, at 41.7°N", *J. Geophys. Res.*, Submitted, 2000.
47. M. Gadsden and W. Schroder, "Noctilucent Clouds", Springer-Verlag, New York, NY, pp. 190, 1989.
48. G.E. Thomas and J.J. Olivero, "Climatology of polar mesospheric clouds, 2. Further analysis of Solar Mesosphere Explorer data", *J. Geophys Res. 94*, pp. 14673–14681, 1989.
49. L. Thomas, A.K.P. Marsh, D.P. Wareing and M.A. Hassan, "Lidar observations of ice crystals associated with noctilucent clouds at middle latitudes", *Geophys. Res. Lett. 21*, pp. 385–388, 1994.
50. G.E. Thomas, "Is the polar mesosphere the miner's canary of global change?", *Adv. Space Res. 18*, pp. (3)49–(3)58, 1996.
51. A.H. Manson, C.E. Meek, H. Teitelbaum, F. Vial, R. Schminder, D. Kurschner, M.J. Smith, G.J. Fraser and R.R. Clark, "Climatologies of semi-diurnal and diurnal tides in the middle atmosphere (70–110 km) at middle latitudes (40–55)", *J. Atmos. Terr. Phys. 51*, pp. 579–593, 1989.
52. R.J. Sica, S. Sargoytchev, P.S. Argall, E.F. Borra, L. Girard, C.T. Sparrow and S. Flatt, "Lidar measurements taken with a large-aperture liquid mirror. 1. Rayleigh-scatter system", *Appl. Optics 34*, pp. 6925–6936, 1995.
53. R.G. Roble and E.C. Ridley, "A thermosphere-ionosphere-mesosphere-electrodynamics general circulation model (time-GCM): Equinox solar cycle minimum simulations (30-500 km)", *Geophys. Res. Lett. 21*, pp. 417–420, 1994.
54. R.G. Roble, "The NCAR thermosphere-ionosphere-mesosphere-electrodynamics general circulation model (TIME-GCM)", in *STEP: Handbook of ionospheric models*, edited by R.W. Schunk, USU/SCOSTEP, Logan, pp. 281–288, 1996.
55. R. Wilson, M.-L. Chanin and A. Hauchecorne, "Gravity waves in the middle atmosphere observed by Rayleigh lidar. 1. Case Studies", *J. Geophys. Res. 96*, pp. 5153–5167, 1991.
56. R. Wilson, M.-L. Chanin and A. Hauchecorne, "Gravity waves in the middle atmosphere observed by Rayleigh lidar. 2. Climatology", *J. Geophys. Res. 96*, pp. 5169–5183, 1991.
57. A.K.P. Marsh, N.J. Mitchell and L. Thomas, "Lidar studies of stratospheric gravity-wave spectra", *Planet. Space Sci 39*, pp. 1541–1548, 1991.
58. J.A. Whiteway and A.I. Carswell, "Lidar observations of gravity wave activity in the upper stratosphere over Toronto", *J. Geophys. Res. 100*, pp. 14113–14124, 1995.

59. R.D. Sears, T.D. Wilkerson, V.B. Wickwar, J.M. Maloney, and S.C. Collins, “Multi-dimensional power spectral analysis of structure in the stratosphere and mesosphere observed by Rayleigh scatter lidar”, in *Advances in Atmospheric Remote Sensing with Lidar*, edited by A. Ansmann, R. Neuber, P. Rairoux, and U. Wandinger, Springer Verlag, Berlin, pp. 561–564, 1997.
60. X. Gao, J.W. Meriwether, V.B. Wickwar, T.D. Wilkerson and S.C. Collins, “Rayleigh lidar measurements of the temporal frequency and vertical wavenumber spectra in the mesosphere over the Rocky Mountain region”, *J. Geophys. Res. 103*, pp. 6405–6416, 1998.
61. K.C. Beissner, Studies of mid-latitude mesospheric temperature variability and its relationship to gravity waves, tides, and planetary waves, Ph.D. thesis, Utah State University, Logan, UT, 1997.
62. M.E. Hagan, J.M. Forbes and F. Vial, “On modeling migrating solar tides”, *Geophys. Res. Lett. 22*, pp. 893–896, 1995.
63. U. von Zahn, G. von Cossart, J. Fiedler, K.H. Fricke, G. Nelke, G. Baumgarten, D. Rees, A. Hauchecorne and K.Adolfsen, “The ALOMAR Rayleigh/Mie/Raman lidar: objectives, configuration, and performance”, *Ann. Geophysicae 18*, pp. 815–833, 2000.
64. U. von Zahn and J. Höffner, “Mesopause temperature profiling by potassium lidar”, *Geophys. Res. Lett. 23*, pp. 141–144, 1996.
65. U. von Zahn, J. Höffner, V. Eska and M. Alpers, “The mesopause altitude: Only two distinctive levels worldwide?”, *Geophs. Res. Lett. 23*, pp. 3231–3234, 1996.
66. V. Eska and J. Höffner, “Observed linear and nonlinear K layer response”, *Geophys Res. Lett. 25*, pp. 2933–2936, 1998.
67. R.E. Bills, C.S. Gardner and C.-Y. She, “Narrowband lidar technique for sodium temperature and Doppler wind observations of the upper atmosphere”, *Opt. Eng. 30*, pp. 13–21, 1991.
68. J. Yu, R. States, S.J. Franke, C.S. Gardner and M. Hagan, “Observations of tidal temperature and wind perturbations in the mesopause region above Urbana, IL (40°N, 88°W)”, *Geophys Res. Lett. 24*, pp. 1207–1210, 1997.
69. P.S. Argall, O.N. Vassiliev, R.J. Sica and M.M. Mwangi, “Lidar measurements taken with a large-aperture liquid mirror. 2. Sodium resonance-fluorescence system”, *Appl. Opt. 39*, pp. 2393–2400, 2000.
70. J.M.C. Plane, C.S. Gardner, J. Yu, C.Y. She, R.R. Garcia and H.C. Pumphrey, “Mesospheric Na layer at 40°N: Modeling and observations”, *J. Geophys. Res. 104*, pp. 3773–3788, 1999.
71. G. Megie, “Laser Measurements of Atmospheric Trace Constituents”, in *Laser Remote Chemical Analysis*, edited by R.M. Measures, John Wiley & Sons, New York, NY, pp. 333, 1988.
72. C.S. Gardner, “Sodium resonance fluorescence lidar applications in atmospheric science and astronomy”, *Proc. IEEE 77*, pp. 408–418, 1989.
73. D. Rees, M. Vyssogorets, N.P. Meridith, E. Griffin and Y. Chaxell, “The Doppler wind and temperature system of the ALOMAR lidar facility: overview and initial results”, *J. Atmos. Terr. Phys. 58*, pp. 1827–1842, 1996.